# Planar faults in layered Bi-containing perovskites studied by X-ray diffraction line profile analysis

Alexandre Boulle, Caroline Legrand, René Guinebretière, Jean-Pierre Mercurio, Alain Dauger

# Planar faults in layered Bi-containing perovskites studied by X-ray diffraction line profile analysis

A. Boulle,[a] C. Legrand,[b] R. Guinebretière,[a*] J. P. Mercurio[b] and A. Dauger[a]

[a]Science des Procédés Céramiques et de Traitements de Surface, UMR 6638, ENSCI, 47-73 avenue Albert Thomas, 87065 Limoges CEDEX, France,
[b]Science des Procédés Céramiques et de Traitements de Surface, UMR 6638, Faculté des Sciences, 123 avenue Albert Thomas, 87060 Limoges CEDEX, France. Correspondence e-mail: r.guinebretiere@ensci.fr

Profile fitting procedures associated with integral breadth studies and Fourier analysis are applied to the study of the complex Bi-containing layered perovskite $SrBi_2Nb_2O_9$. Strong line broadening anisotropy is evidenced. Both 'size' and 'strain' effects contribute to the observed width. However, 'size' broadening along the [00*l*] direction is essentially caused by stacking faults. The coherently diffracting domain sizes are deduced from Fourier analysis of the diffraction patterns and a rough estimate of the mean distance between faults is given. Thermal annealing significantly decreases the stacking fault density.

## 1. Introduction

Since the early 1990s, great attention has been paid to ferroelectric thin films for non-volatile random access memory application. For this type of application, the Aurivillius compound $SrBi_2Nb_2O_9$ (SBN) is a potential candidate because of its excellent resistance to polarization fatigue (Desu & Vijay, 1989). Aurivillius compounds are a family of oxide materials composed of stacked $A_{m-1}B_mO_{3m+1}$ 'perovskite like' layers separated by $Bi_2O_2$ slabs (Aurivillius, 1949). The 'perovskite like' block can adopt various thicknesses with respect to the number *m*. Different stacking polytype structures have been reported with *m* ranging between 1 and 5. In the case of SBN, *m* equals 2. This regular arrangement along the [001] direction may be violated, giving rise to local changes of the *m* value. Such behaviour is well known in similar bismuth-containing layered perovskites (Balzar, 1993; Balzar & Ledbetter, 1992). The ferroelectric properties (*e.g.* polarization and coercive field) of such compounds depend on the thickness of the perovskite layer (Du & Chen, 1998). In addition, such defects reduce the spatial extent over which diffraction is coherent, thus producing line broadening.

Broadening of X-ray diffraction lines arises on the one hand from geometrical aberrations and radiation wavelength distribution, and on the other hand from crystalline imperfections (finite grain size, microstrains, stacking faults, *etc.*) (Klug & Alexander, 1974). In this work, we use pattern decomposition combined with line profile analysis to investigate the microstructure of a complex compound. The X-ray diffraction effects of stacking faults in sol–gel derived SBN powders are considered.

## 2. Experimental

### 2.1. Synthesis

An appropriate SBN precursor solution was prepared by dissolution of strontium 2-ethylhexanoate in 2-ethylhexanoic acid at 393 K, followed by addition of bismuth 2-ethylhexanoate, and finally addition of niobium ethoxide, previously dissolved in ethanol. SBN powders were obtained after conventional drying and heat treatment at 973 K for various durations (from 0.5 to 600 h). Thin films were fabricated by spinning the precursor solution at 4000 r.p.m. for 30 s (using a Sulzer photoresist spinner) on single-crystalline (100) $SrTiO_3$ substrates. Details concerning the characteristics of the whole process have been published elsewhere (Yi, 1998).

### 2.2. Data collection

X-ray diffraction experiments were performed on a home-made high-resolution setup (Masson, 1998). The primary linear beam was supplied by a rotating anode source. Monochromatic ($\Delta\lambda/\lambda = 1.4 \times 10^{-4}$) and parallel ($\Delta\theta = 12''$) Cu $K\alpha_1$ X-rays were obtained using a four-bounce Ge monochromator in the (220) setting. Samples were positioned on a high-precision five-axis sample holder in a vacuum chamber. Sample positioning was performed by using the diffracted beams of a single-crystalline sample holder. The specimens were studied under fixed incidence in asymmetric geometry and were continuously rotated about their surface normal during the experiment. A representative diffraction pattern of a sample annealed for 10 h at 973 K is given in Fig. 1.

At $2\theta$ angles above 10–15°, the instrumental profile is symmetric; it is well described by a Voigt function and the line breadth and shape can be deduced by considering only four meaningful parameters: focal spot size, equatorial divergence, wavelength spread and the transfer function of the detector (Masson *et al.*, 1998). Below 10° incidence, the breadth of the instrumental profile, $\beta_g$, ranges between 0.07 and 0.11° (see also Fig. 2). Below $2\theta$ = 10–15°, the instrumental profile is slightly asymmetric as a result of axial divergence (Masson *et al.*, 2001). In the present, study this effect is not considered, since no diffraction line of interest occurs in this range. Anyway, this effect is well known and may be easily accounted

for by using appropriate corrections (Masson *et al.*, 2001; Finger *et al.*, 1994).

### 2.3. Line profile analysis

Line profile analysis has been carried out using integral breadth methods and Fourier analysis. The experimental profiles were modelled with a Voigt function. The main drawback of these methods is that results are biased by rather restrictive hypotheses: the so-called Stokes & Wilson (1944) approximation for the integral breadth methods and a truncated Taylor series in the Warren–Averbach method (Warren, 1969). Nevertheless, the classical methods are widely used (see *e.g.* Langford, 1999; Louër, 1999) and were shown to be powerful in very similar studies (Scardi *et al.*, 1993, 1997; Balzar, 1993). Because of their general applicability without restriction to specific crystal systems, these methods are well suited to the study of complex compounds exhibiting many different microstructural features.

**2.3.1. Removal of instrumental broadening**. The characterization of the microstructural properties of the specimen with the above-mentioned methods requires the integral breadths $\beta_f$ of the profile $f(x)$ arising from the microstructure of the sample. The $f(x)$ profile can be obtained by the inversion of the equation $h(x) = f(x)*g(x)$, where $h(x)$ and $g(x)$ are the experimental and instrumental profiles, respectively, and * denotes the convolution. In the case of complicated patterns showing a high degree of line overlap, this inversion is more easily carried out by making the assumption that $h(x)$ and $g(x)$ are described by a suitable analytical function (Klug & Alexander, 1974). Using the Voigt function, one obtains

$$\beta_{f_L} = \beta_{h_L} - \beta_{g_L} \quad \text{and} \quad \beta_{f_G}^2 = \beta_{h_G}^2 - \beta_{g_G}^2, \tag{1}$$

where the subscripts $L$ and $G$ denote the Lorentzian and Gaussian components, respectively. The result of a fitting by means of a Voigt function to a cluster of two lines is shown in the inset of Fig. 1.

**2.3.2. Integral breadth method**. The breadths $\beta_{f_L}$ and $\beta_{f_G}$ are the Gaussian and Lorentzian breadths of the Voigt function. In the method introduced by Langford (1978, 1992), the Lorentzian and Gaussian breadths expressed in reciprocal space ($\beta^* = \beta\cos\theta/\lambda$) are analysed separately as a function of the length of the diffraction vector:

$$\beta_{f_L}^* = \beta_{S_L}^* + \frac{\eta_L}{2} d^* \quad \text{and} \quad \beta_{f_G}^{*2} = \beta_{S_G}^{*2} + \left(\frac{\eta_G}{2}\right)^2 d^{*2}, \tag{2}$$

where the subscript $S$ refers to the size contribution to line breadth. $\beta_{S_L}^*$, $\beta_{S_G}^*$ and $\eta_L$, $\eta_G$ are combined (Langford, 1992) and give, respectively, a measure of the volume-averaged domain size $\langle D\rangle_V$ and apparent strain $\eta$. However, as pointed out by Langford *et al.* (2000), the derived quantities used to describe microstructural properties are model dependent. Therefore, the results should often be regarded as educated guesses, unless they are confirmed by complementary experiments (*e.g.* electron microscopy) or by using physically meaningful microstructural models, if available.

**2.3.3. Fourier analysis**. The above-mentioned method yields average values. Size and strain distribution can be computed by a Fourier analysis of the diffraction lines (Warren, 1969). However, in its original form, this method is restricted to materials with high symmetry, because of the lack of peak overlap in such cases. In practice, this method is thus rarely usable, unless peak tails are cut or approximate. To overcome the peak overlap problem and hence to extend this method to materials with lower symmetries, many authors have combined the profile fitting method with the Warren–Averbach method (Enzo *et al.*, 1988; Scardi *et al.*, 1991; Scardi & Leoni, 1999; Balzar, 1993; Audebrand *et al.*, 1998, 2000). This also enables one to use the deconvolution method described above, thus avoiding the method of Stokes (1948), which often leads to spurious effects or unstable solutions, especially when sample broadening is low. Fourier coefficients of the physically broadened line profile are calculated analytically using the

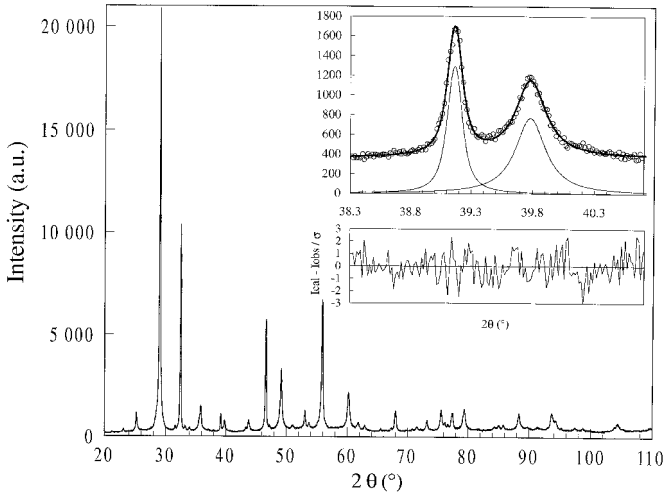


**Figure 1**
X-ray diffraction diagram of an SBN powder annealed for 10 h at 973 K. Inset: fit of a cluster of two lines using Voigt functions (GoF = 1.11, $R_p$ = 3.53%).

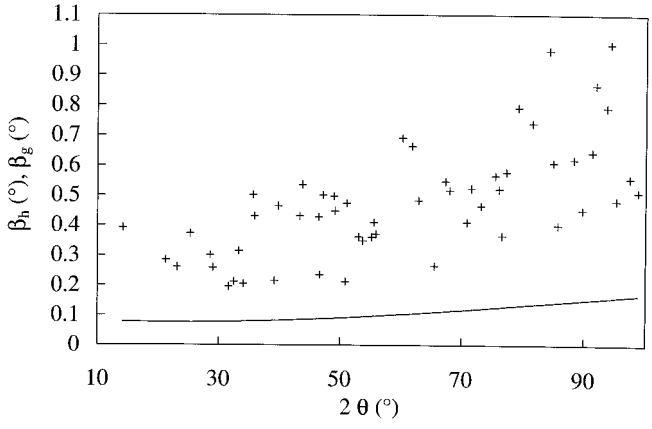


**Figure 2**
Plot of the observed integral breadth $\beta_h$ (+) and the breadth of the instrumental profile (—) *versus* the diffraction angle. A significant sample contribution to line broadening is observed.

breadths $\beta_{f_L}$ and $\beta_{f_G}$ (Balzar, 1999). The size coefficient $A_S(L)$ and the mean squared strain $\langle e^2(L)\rangle$ can be separated by means of (Delhez & Mittemeijer 1976)

$$A(L, d^*) = A_S(L)\left[1 - 2\pi^2 d^{*2} L^2 \langle e^2(L)\rangle\right], \qquad (3)$$

where $L$ is the correlation length. However, as pointed out by many authors (*e.g.* Langford *et al.*, 2000), the Fourier coefficients used in this method are those of the Voigt function representing the profile and not those of the profile itself. Hence the shape of the calculated domain size distribution depends on the chosen profile (*i.e.* the true shape remains unknown). Nevertheless, diffraction profiles are not very sensitive to fine details of the distribution, but rather to the mean and width (Rao & Houska, 1986*a*,*b*). Calculated distributions may thus provide a qualitative view of the mean and width of the domain size distribution. In any case, unreliable results are obtained if the observed profiles are incorrectly modelled.

All multiple-line methods require at least two orders of reflection. In the case of SBN powders, the number of observable 00*l* reflections lies between 3 and 5 over a 50° $2\theta$ range, depending on the relative intensities and the degree of line overlap. Hence, even though such lines are of rather weak intensity and are often strongly overlapped, satisfactory results can be extracted.

## 3. Results

### 3.1. Generalities

All peaks of the pattern shown in Fig. 1 can be indexed in the orthorhombic phase of SBN. The orthorhombic distortion is very small since $a/b$ equals 1.00063 (space group $A2_1am$, JCPDS card No. 86-1190). The $2\theta$ difference between the ($h$00) and (0$k$0) lines is smaller than 0.001°. These lines can hence be modelled with one single profile (Balzar, 1993; Balzar & Ledbetter, 1992). A comparison of the breadth of the observed profile and the instrumental profile is presented in Fig. 2. It is clear from this figure that the sample contribution

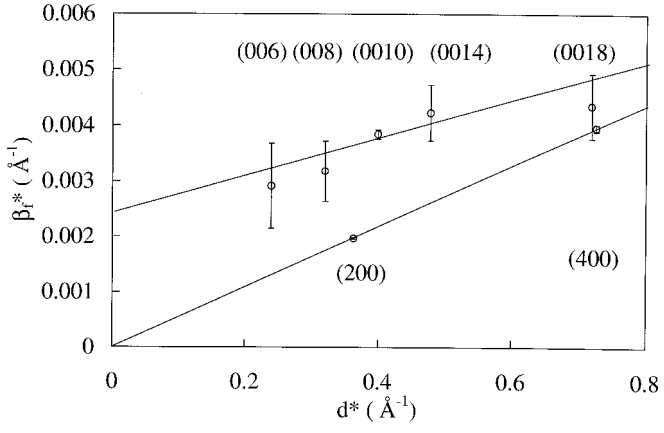


**Figure 3**
Williamson–Hall plot for the 00*l* and *h*00 lines. Size broadening is much more pronounced along the *c* axis than along the *a* axis. The powder has been annealed for 10 h at 973 K.

**Table 1**
Breadth and shape factor data for several reflections.

The breadths are given in degrees. In the **c** direction, the profiles are Lorentzian, whereas a Voigtian line shape is observed along directions in the *ab* plane.

| $2\theta$ (°) | *hkl* | $\beta_{f_G}$ | $\beta_{f_L}$ | $\beta_f$ | $\varphi$ |
|---|---|---|---|---|---|
| 28.502 | 008 | 0 | 0.176 | 0.176 (18) | 0.636 (26) |
| 32.461 | 200 | 0.088 | 0.114 | 0.171 (2) | 0.745 (2) |
| 35.831 | 0010 | 0.007 | 0.335 | 0.335 (8) | 0.637 (11) |
| 43.306 | 0012 | 0.015 | 0.261 | 0.261 (41) | 0.637 (57) |
| 46.567 | 220 | 0.105 | 0.149 | 0.216 (2) | 0.736 (3) |
| 50.993 | 0014 | 0.005 | 0.456 | 0.456 (42) | 0.637 (59) |
| 67.269 | 0018 | 0.015 | 0.350 | 0.350 (40) | 0.637 (57) |
| 67.985 | 400 | 0.157 | 0.325 | 0.407 (7) | 0.698 (10) |
| 77.379 | 240 | 0.231 | 0.276 | 0.431 (13) | 0.754 (18) |

to line broadening is significant. Moreover, the strong scatter of experimental data indicates a marked *hkl* dependence of the $f(x)$ profile.

### 3.2. Williamson–Hall plot

To ascertain that the line breadths effectively depend on the diffraction vector, we plotted $\beta_f$ as a function of $d^*$ in a Williamson–Hall plot (Williamson & Hall, 1953) for the 00*l* and *h*00 reflections of the sample that had been annealed for 10 h at 973 K (see Fig. 3). The $\beta_f$ line for the 00*l* reflection has non-zero intercept and slope, indicating a marked size effect (*i.e.* order-independent broadening) and the presence of microstrains (order-dependent broadening). For the *h*00 line, the intercept is almost nil (*i.e.* no size broadening) and the slope is non-zero. Since stacking faults occur along the [00*l*] direction, the *h*00 reflections are not affected. For those lines, the zero intercept indicates rather coarse domains. On the other hand, the 00*l* lines are directly affected by faulting, as attested by the significant size effect.

### 3.3. Line shape

The shape factors $\varphi_f$ (= FWHM$_f$/$\beta_f$) together with the $\beta$ data of the two above-cited groups of reflections are given in Table 1. Firstly, all $\varphi$ data lie between the Lorentzian (0.636) and the Gaussian (0.939) limits. Secondly, it appears that the 00*l* lines exhibit a purely Lorentzian line shape, whereas the *h*00 reflections have a greater Gaussian component. As will be seen below, this is in good agreement with the presence of faults along the [00*l*] direction.

## 4. Discussion

### 4.1. Stacking faults

Defects consisting of coherently diffracting domains shifted with respect to one another (which in SBN corresponds to a local variation of the $m$ value) have been described by Van Berkum *et al.* (1996) as highly localized strain fields. The corresponding line profiles exhibit slowly decaying tails (*i.e.* strong Lorentzian character) and strong 'order-independent' broadening. However, a contribution to microstrains is not excluded since pure 'order-independent' broadening is

obtained for the extreme case of infinitely narrow strain fields. Several authors have observed the same tendency for analogous defects (Balzar, 1993; Balzar & Ledbetter, 1992; Scardi *et al.*, 1993, 1997). They related the apparent domain size $D$ to the contribution of stacking faults $D_F$ using the equation derived by Warren (1969) for in-plane translation stacking faults, in the case of low fault percentage:

$$1/\langle D\rangle_S = 1/\langle D_C\rangle_S + 1/\langle D_F\rangle_S, \quad (4)$$

where $\langle \ldots \rangle_S$ designates an area average and $D_C$ is the real crystal size (limited by the surface of the grains). In general, the observed size profile is the convolution of the profile $f_S(x)$ arising from the crystallite size and $f_{SF}(x)$ resulting from stacking faults:

$$f(x) = f_S(x) * f_{SF}(x). \quad (5)$$

For the sample annealed for 10 h at 973 K, the calculation of the domain size using Langford's method yields 182 (56) and 33 (2) nm in the [$h$00] and [00$l$] directions, respectively. This confirms the high anisotropy deduced from the Williamson–Hall plot. The same treatment was performed for other directions ([111], [113], [115], [117]). The behaviour of the apparent size could not be related to a simple crystal shape (Langford *et al.*, 1993). The observed size anisotropy was hence attributed to the presence of faults perpendicular to the $c$ axis.

Lorentzian-shaped profiles have been frequently observed in stacking-fault-containing crystals, though this is not a general rule (Ustinov, 1999). Wilson (1961) calculated the line profile of stacking-fault-containing crystals. In the case of close-packed structures, the profiles are approximately Lorentzian. This has been confirmed by Langford *et al.* (1993) for ex-oxalate ZnO. The same trend has been observed for stacking faults analogous to those expected in SBN. Balzar (1993) and Balzar & Ledbetter (1992) studied a Bi–Cu–O superconductor that possessed a very similar structure to that of SBN (perovskite units separated by $Bi_2O_2$ slabs). They showed that such compounds may contain stacking faults that give rise to 'order-independent' broadening. Although they

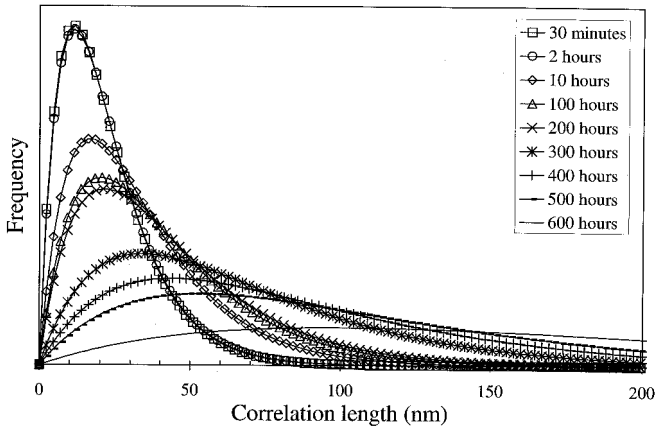


**Figure 4**
Volume-weighted domain size distribution for several annealing conditions.

**Table 2**
Results of Fourier analysis.

The subscripts $S$ and $V$ refer to surface and volume weights, respectively. The root-mean-square strain is taken at $\langle D\rangle_S/2$. $\langle D_F\rangle_V$ is the calculated mean distance between faults.

| Annealing duration (h) | $\langle D\rangle_S$ (nm) | $\langle D\rangle_V$ (nm) | $\langle e^2\rangle^{1/2}$ (%) | $\langle D_F\rangle_V$ (nm) |
|---|---|---|---|---|
| 0.5 | 11 (1) | 22 (2) | 0.23 (8) | 31 (2) |
| 2 | 11 (1) | 22 (2) | 0.27 (6) | 31 (2) |
| 10 | 16 (1) | 33 (2) | 0.17 (5) | 47 (2) |
| 100 | 20 (2) | 40 (3) | 0.16 (3) | 57 (3) |
| 200 | 22 (2) | 45 (5) | 0.15 (2) | 65 (5) |
| 300 | 32 (2) | 64 (4) | 0.16 (2) | 89 (4) |
| 400 | 43 (6) | 85 (13) | 0.16 (1) | 118 (13) |
| 500 | 52 (20) | 104 (40) | 0.14 (4) | 149 (40) |
| 600 | 98 (10) | 198 (20) | 0.03 (1) | 282 (20) |

did not give the values of the shape factors, they always obtained a Lorentzian width that was much greater than the Gaussian width. It is possible to calculate the shape factor on the basis of the Lorentzian and Gaussian components (de Keijser *et al.*, 1982; Delhez *et al.*, 1982); the calculation yields 0.641, 0.717 and 0.677 depending on the composition. These values are very close to the Lorentzian limit of the shape factor (0.636), attesting that such stacking faults also yield a Lorentzian shape. Simulation of X-ray diffraction diagrams leads to the same conclusions (Nuttall & Day, 1999). Hence, both line shape and width anisotropy show the presence of planar faults perpendicular to the [00$l$] direction.

### 4.2. Effect of thermal annealing

SBN powders were further annealed at 973 K. Results of the line profile analysis are given in Table 2. For the sake of briefness, we present the results of the Fourier analysis only. The value of the root-mean-square strain is taken at $\langle D\rangle_S/2$ (Klug & Alexander, 1974). It can be seen that increasing the thermal annealing time results in a significant lowering of sample imperfections. In particular, the coherently diffracting domain size increases markedly. The volume-weighted domain size is twice the surface-weighted domain size, which corresponds to the Lorentzian limiting case (Balzar, 1999). Line overlap is here too severe to measure subtle variations of the shape factor in the [00$l$] direction. However, similar experiments have been performed on epitaxial layers (Boulle *et al.*, 2001). In such cases, the diffraction lines were well separated and reductions of the Lorentzian content were detected. The domain size distributions are given in Fig. 4. The maximum of the distribution is shifted towards high $L$ values and the distribution becomes much broader.

Since the profiles are purely Lorentzian, equation (5) may be rewritten as

$$1/\langle D\rangle_V = 1/\langle D_C\rangle_V + 1/\langle D_F\rangle_V. \quad (6)$$

Hence, knowing the crystal size $\langle D_C\rangle_V$, it should be possible to calculate the mean distance between stacking faults. According to the high cell-parameter anisotropy, the shape of the crystal is unlikely to be isotropic. Consequently, the value of the apparent domain size in the [$h$00] direction cannot be

used as a measure of the real crystal size in the [00*l*] direction. We shall therefore assume that all grains are faulted. The maximum $L$ value (say, corresponding to 99% of the cumulative distribution) may thus be regarded as the crystal size. The calculation is now straightforward; results are given in Table 2. The stacking fault density is lowered as heat treatment time is increased. The rather unrealistic values obtained after long duration seem to indicate that the specimens are almost free of faults. The stacking sequence has reached its equilibrium configuration.

## 5. Conclusion

X-ray diffraction line profile analysis methods have been applied to the study of a complex compound exhibiting stacking disorder. Profile fitting procedures associated with integral breadth analysis revealed strong anisotropic line broadening. This broadening contains both 'size' and 'strain' contributions. In the [00*l*] direction, 'size' broadening is mainly the result of stacking faults. Profile fitting techniques associated with Fourier analysis enabled the computation of the domain size distributions in this direction. When SBN powders are thermally annealed, the stacking fault density is lowered. Prolonged annealing (*e.g.* 600 h) results in specimens that are almost free of faulting.

## References


Audebrand, N., Auffredic, J. P. & Louër, D. (1998). *Chem. Mater.* **10**, 2450–2461.

Audebrand, N., Auffredic, J. P. & Louër, D. (2000). *Chem. Mater.* **12**, 1791–1799.

Aurivillius, B. (1949). *Arkiv. Kemi.* **1**, 499–512.

Balzar, D. (1993). *J. Res. Natl Inst. Stand. Technol.* **98**, 321–353.

Balzar, D. (1999). *Defect and Microstructure Analysis by Diffraction*, edited by R. L. Snyder, J. Fiala & H. J. Bunge, pp. 94–126. Oxford University Press.

Balzar, D. & Ledbetter, H. (1992). *J. Mater. Sci. Lett.* **11**, 1419–1420.

Boulle, A., Legrand, C., Guinebretière, R., Mercurio, J. P. & Dauger, A. (2001). *Thin Solid Films*, **391**, 42–46.

Delhez, R., de Keijser, Th. H. & Mittemeijer, E. J. (1982). *Fresenius Z. Anal. Chem.* **312**, 1–16.

Delhez, R. & Mittemeijer, E. J. (1976). *J. Appl. Cryst.* **9**, 233–234.

Desu, S. B. & Vijay, D. P. (1989). *Science*, **246**, 1400.

Du, X. & Chen, I. W. (1998). *J. Am. Ceram. Soc.* **81**, 3260–3265, 3265–3269.

Enzo, S., Fagherazzi, G., Benedetti, A. & Polizzi, S. (1988). *J. Appl. Cryst.* **21**, 536–542.

Finger, L. W., Cox, D. E. & Jephcoat, A. P. (1994). *J. Appl. Cryst.* **27**, 892–900.

Keijser, Th. H. de, Langford, J. I., Mittemeijer, E. J. & Vogels, A. B. P. (1982). *J. Appl. Cryst.* **15**, 308–314.

Klug, H. P. & Alexander, L. E. (1974). *X-ray Diffraction Procedures for Polycrystalline and Amorphous Materials*. New York: John Wiley.

Langford, J. I. (1978). *J. Appl. Cryst.* **11**, 10–14.

Langford, J. I. (1992). *Natl Inst. Stand. Technol. Spec. Pub.* **846**, 110–126.

Langford, J. I. (1999). *Defect and Microstructure Analysis by Diffraction*, edited by R. L. Snyder, J. Fiala & H. J. Bunge, pp. 94–126, 59–81. Oxford University Press.

Langford, J. I., Boultif, A., Auffrédic, J. P. & Louër, D. (1993). *J. Appl. Cryst.* **26**, 22–33.

Langford, J. I., Louër, D. & Scardi, P. (2000). *J. Appl. Cryst.* **33**, 964–974.

Louër, D. (1999). *Defect and Microstructure Analysis by Diffraction*, edited by R. L. Snyder, J. Fiala & H. J. Bunge, pp. 94–126, 673–697. Oxford University Press.

Masson, O. (1998). Thesis, University of Limoges, France.

Masson, O., Guinebretière, R. & Dauger, A. (1998). *Mater. Sci. Forum*, **278–281**, 115–120.

Masson, O., Guinebretière, R. & Dauger, A. (2001). *J. Appl. Cryst.* **34**, 436–441.

Nuttall, C. J. & Day, P. (1999). *J. Solid State Chem.* **147**, 3–10.

Rao, S. & Houska, C. R. (1986*a*). *Acta Cryst.* A**46**, 6–13.

Rao, S. & Houska, C. R. (1986*b*). *Acta Cryst.* A**46**, 14–19.

Scardi, P., Kothari, D. C. & Guzman, L. (1991). *Thin Solid Films*, **195**, 213–223.

Scardi, P., Lutterotti, L., Correra, L. & Nicoletti, S. (1993). *J. Mater. Res.* **8**, 2780–2784.

Scardi, P., Matacotta, F. C., Dediu, V. I. & Correra, L. (1997). *J. Mater. Res.* **12**, 28–37.

Scardi, P. & Leoni, M. (1999). *J. Appl. Cryst.* **32**, 671–682.

Stokes, A. R. (1948). *Proc. Phil. Soc. London Ser. A*, **61**, 382–391.

Stokes, A. R. & Wilson, A. J. C. (1944). *Proc. Phys. Soc.* **56**, 174–181.

Ustinov, A. I. (1999). *Defect and Microstructure Analysis by Diffraction*, edited by R. L. Snyder, J. Fiala & H. J. Bunge, pp. 264–317. Oxford University Press.

Van Berkum, J. G. M., Delhez, R., de Keijser, Th. H., Mittemeijer, E. J. (1996). *Acta Cryst.* A**52**, 730–747.

Warren, B. E. (1969). *X-ray Diffraction*. New York: Addison-Wesley.

Williamson, G. K. & Hall, W. H. (1953). *Acta Metall.* **1**, 22–31.

Wilson, A. J. C. (1962). *X-ray Optics*, 2nd ed. London: Methuen.

Yi, J. H. (1998). Thesis, University of Limoges, France.